Observation of non-principal plane neutral points in the in-water upwelling polarized light field

Kenneth J. Voss,[1,*] Arthur C. R. Gleason,[1] Howard R. Gordon, [1] George W. Kattawar, [2] and Yu You[2]

[1]*Physics Department, University of Miami, 1320 Campo Sano Dr., Coral Gables, Fl, 33146, USA*
[2] *Physics and Astronomy Department, Texas A&M University, College Station, Tx. 77843-4242, USA*
**voss@physics.miami.edu*

Abstract: Neutral points are specific directions in the light field where the three Stokes parameters *Q*, *U*, *V*, and thus the degree of polarization simultaneously go to zero. We have made the first measurement of non-principal-plane neutral points in the upwelling light field in natural waters. These neutral points are located at approximately 40°- 80° nadir angle and between 120° - 160° azimuth to the sun which is well off of the principal plane. Calculations show that the neutral point positions are very sensitive to the balance in the incident light between the partially polarized skylight and the direct solar beam.

OCIS codes: (010.4450) Oceanic optics; (010.4458) Oceanic scattering; (260.5430) Polarization.

References and links

1. K. L. Coulson, *Polarization and intensity of light in the Atmosphere* (A. Deepak Publishing, Hampton, VA, 1988).
2. G. Horvath, B. Bernath, B. Suhai, A. Barta, and R. Wehner, "First observation of the fourth neutral polarization point in the atmosphere," J. Opt. Soc. Am. A **19**(10), 2085–2099 (2002).
3. J. Babinet, "Sur un nouveau point neutre dans l'atmosphere," CR (East Lansing, Mich.) **11**, 618–620 (1840).
4. D. Brewster, "On the polarisation of the atmosphere," Phil. Mag. J. Sci. **31**, 444–454 (1847).
5. M. J. L. Soret, "Influence des surfaces d'eau sur la polarisation atmospherique et observation de deux points neutres a droite et a gauche de Soleil," Compt. Rend. **107**, 867–870 (1888).
6. R. S. Fraser, "Atmospheric neutral points over water," J. Opt. Soc. Am. **58**(8), 1029–1031 (1968).
7. M. A. Cornu, "Observations relatives a la couronne visible actuellement autour du Soleil," Compt. Rend. **99**, 488–493 (1884).
8. J. T. Adams, and G. W. Kattawar, "Neutral points in an atmosphere-ocean system. 1: Upwelling light field," Appl. Opt. **36**(9), 1976–1986 (1997).
9. Y. Kawata, and A. Yamazaki, "Multiple scattering analysis of airborne POLDER image data over the sea," IEEE Trans. On Geoscience Remote Sens. **361**1), 51–60 (1998).
10. C. F. Bohren, and D. R. Huffman, *Absorption and Scattering of Light by Small Particles* (John Wiley and Sons, New York, NY, 1983).
11. A. Ivanoff, and T. H. Waterman, "Elliptical polarization of submarine illumination," J. Mar. Res. **16**, 255–282 (1958).
12. K. J. Voss, and N. Souaidia, "POLRADS: polarization radiance distribution measurement system," Opt. Express **18**(19), 19672–19680 (2010).
13. K. J. Voss, and A. L. Chapin, "Upwelling radiance distribution camera system, NURADS," Opt. Express **13**(11), 4250–4262 (2005).
14. H. R. Gordon, and K. Ding, "Self-shading of in-water optical instruments," Limnol. Oceanogr. **37**(3), 491–500 (1992).
15. P.-W. Zhai, G. W. Kattawar, and P. Yang, "Impulse response solution to the three-dimensional vector radiative transfer equation in atmosphere-ocean systems. I. Monte Carlo method," Appl. Opt. **47**(8), 1037–1047 (2008).
16. P. M. Teillet, "Rayleigh optical depth comparisons from various sources," Appl. Opt. **29**(13), 1897–1900 (1990).
17. S. Pegau, J. R. V. Zaneveld, B. G. Mitchell, J. L. Mueller, M. Kahru, J. Wieland, and M. Stramska, "Ocean Optics Protocols For Satellite Ocean Color Sensor Validation, Revision 4, Volume IV: Inherent Optical Properties: Instruments, Characterizations, Field Measurements, and Data Analysis Protocols," NASA/TM-2003–21621/Rev4-Vol IV (Goddard Space Flight Center, Greenbelt, MD, 2002).
18. A. Morel, and B. Gentili, "Diffuse reflectance of oceanic waters: its dependence on Sun angle as influenced by the molecular scattering contribution," Appl. Opt. **30**(30), 4427–4438 (1991).

#138994 - $15.00 USD Received 30 Nov 2010; revised 18 Feb 2011; accepted 8 Mar 2011; published 16 Mar 2011

19. K. J. Voss, and E. S. Fry, "Measurement of the Mueller matrix for ocean water," Appl. Opt. **23**(23), 4427–4439 (1984).
20. T. J. Petzold, "Volume scattering functions for selected ocean waters," SIO Ref. 72–78 (University of California, San Diego, Scripps Institution of Oceanography Visibility Laboratory, 1972).
21. L. G. Henyey, and J. L. Greenstein, "Diffuse radiation in the galaxy," Astrophys. J. **93**, 70–83 (1941).
22. J. T. Adams, E. Aas, N. K. Hjørslev, and B. Lundgren, "Comparison of radiance and polarization values observed in the Mediterranean Sea and simulated in a Monte Carlo model," Appl. Opt. **41**(15), 2724–2733 (2002).
23. J. Lenoble, and C. Broquez, "A comparitive review of radiation aerosol models," Contrib. Atmos. Phys. **57**, 1–20 (1984).
24. C. Cox, and W. Munk, "Statistics of the sea surface derived from sun glitter," J. Mar. Res. **13**, 198–227 (1954).
25. J. Chowdhary, B. Cairns, and L. D. Travis, "Contribution of water-leaving radiances to multiangle, multispectral polarimetric observations over the open ocean: bio-optical model results for case 1 waters," Appl. Opt. **45**(22), 5542–5567 (2006).
26. J. T. Adams, and D. J. Gray, "Neutral points in an atmosphere-ocean system. 2: Downwelling light field," Appl. Opt. **50**(3), 335–346 (2011).

1. Introduction

Neutral points, positions where the light field polarization goes to zero, have been studied since skylight was found to be polarized. A good review of neutral points in the sky can be found in Coulson [1]. Arago discovered that skylight was polarized in 1809 and is also credited with observing the Arago neutral point soon after [1]. This point is located above the anti-solar point, and is observable from the surface only at large solar zenith angles, but from elevated positions it can be seen at smaller solar zenith angles [2]. A second neutral point, the Babinet neutral point, was discovered by Babinet in 1840 [3] and is located near the sun, but above the solar position. A third neutral point, the Brewster point, was discovered by Brewster in 1842 [4] and is located near the sun, but below the solar position. A fourth neutral point, was found by Horvath et al. [2], but is located below the horizon and is only visible from high altitudes, such as from a balloon or space.

These atmospheric neutral points are typically found on the principal plane (the plane containing the solar direction and the zenith direction); however if there is a Fresnel reflecting surface below the observations, such as a quiet lake or an ocean, these neutral points have been found off of the principal plane (found experimentally by Soret [5] and shown theoretically by Fraser [6]). In addition, in cases of high turbidity (volcanic eruption of Krakatoa), Cornu [7] observed neutral points off of the principal plane. The observations by Soret and Cornu are the only two observations that we are aware of in which the neutral points were found off the principal plane in downwelling skylight, but calculations have shown neutral points for upwelling light above an ocean surface that were significantly away from this plane [8] and these have been observed in POLDER data [9].

In this paper we will discuss our experimental results showing neutral points in the upwelling subsurface marine light field, significantly off of the principal plane. These were discovered in measurements performed over two different days, in clear water off of Hawaii. In addition to showing these experimental results, we will show model calculations that, while not exactly reproducing the data, indicate possible sources of these areas of zero, or low, polarization.

2. Stokes Vectors and polarization parameters

The light field polarization is easily described by use of the four parameter Stokes Vector, which has been defined many times, for example in Bohren and Huffman [10]. These four parameters are prescribed relative to some reference plane, in our case we will choose the plane defined by the viewing direction and the nadir direction. Consider an electromagnetic wave of angular frequency ω. If the unit vector $\hat{l}$ is parallel and the unit vector $\hat{r}$ is perpendicular to the reference plane (such that $\hat{r}$ x $\hat{l}$ is in the direction of propagation), the electric field can be written $\vec{E} = E_l \hat{l} + E_r \hat{r}$, with

$$E_\ell = E_{\ell 0} \exp[i(\omega t + \delta_\ell)] \quad (1)$$

#138994 - $15.00 USD Received 30 Nov 2010; revised 18 Feb 2011; accepted 8 Mar 2011; published 16 Mar 2011

$$E_r = E_{r0} \exp[i(\omega t + \delta_r)] \tag{2}$$

where $E_{\ell 0}$ and E_{r0} are real. The Stokes parameters are then defined as:

$$I \equiv E_\ell E_\ell^* + E_r E_r^* = E_{\ell 0}^2 + E_{r0}^2 \tag{3}$$

$$Q \equiv E_\ell E_\ell^* - E_r E_r^* = E_{\ell 0}^2 - E_{r0}^2 \tag{4}$$

$$U \equiv E_\ell E_r^* + E_r E_\ell^* = 2E_{\ell 0} E_{r0} \cos\delta \tag{5}$$

$$V \equiv i(E_\ell E_r^* - E_r E_\ell^*) = 2E_{\ell 0} E_{r0} \sin\delta \tag{6}$$

where $\delta \equiv \delta_r - \delta_\ell$. In our measurements V is assumed negligible in the upwelling light field [11]. Two parameters that we will use in our discussion of neutral points are the degree of linear polarization, *DOP*, and the plane of linear polarization (specified by the angle χ) defined as:

$$DOP = \sqrt{\frac{Q^2 + U^2}{I^2}} \tag{7}$$

$$\tan 2\chi = \frac{U}{Q} \tag{8}$$

As can be seen, neutral points are then defined as locations where both Q and U are simultaneously zero. We should note that there is ambiguity in the literature about these definitions, so one must be very careful to be consistent in their use.

3. Methods

3.1 Measurements

Measurements of the polarized upwelling radiance distribution were accomplished with the PolRADS system [12]. All measurements were done just below the surface, at a depth of 0.5 m. This system was based on the NuRADS camera system [13] and had spectral bands (~10 nm FWHM) centered at 412, 436, 486, 526, 548 and 615 nm. This study did not use data from the 615 nm channel due to the large influence of instrument self-shading at this wavelength resulting from the much higher absorption coefficient of water at this wavelength [14]. In the PolRADS instrument, three NuRADS cameras, each with a linear polarizer in a different orientation, are used to take synchronized images. Typical exposure times were less than one second, however acquiring a set of images from all six wavelengths took about two minutes due to the delay reading the data from the CCD.

Reduction of the raw PolRADS images consisted of applying calibration factors (see [12]) and combining images from the individual, synchronized NuRADS sensors as described in [12]. For some of this analysis, we averaged images in both space and time to reduce environmental noise. Before averaging, each image was inspected to find the anti-solar point, to correct the geometry of the image, and to check for obstructions in the field of view such as fish, the cables, the side of the ship, or other instruments. Images were then averaged in 10-minute bins, excluding those that had been flagged as unacceptable in the inspection stage. The symmetry of the images about the principal plane was exploited to further average both halves of each image. In addition, spatial binning of 3 × 3 pixel windows was performed to produce final average images at 1° × 1° resolution. Each pixel in the processed image for a given band, therefore, could have been an average of up to 90 raw pixels (5 images × 2 image halves × 9 pixel windows). The mean, and coefficient of variation (standard deviation divided by the mean) for the radiance and standard deviation for Q and U were computed for each pixel in the processed image from the up to 90 raw pixels in the original images.

#138994 - $15.00 USD Received 30 Nov 2010; revised 18 Feb 2011; accepted 8 Mar 2011; published 16 Mar 2011

As an output from this processing we obtained the Stokes Vector (*I*, *Q*, *U*, but not *V*), *DOP* and χ. In addition we have the coefficient of variation for *I*, *Q*, and *U*. In an earlier paper we performed an error analysis of this inversion [12], we estimated that the uncertainty in the absolute value of the retrieved *Q/I* and *U/I* was approximately 0.05. The accuracy of determining relative directions in the images is on the order of 1°.

3.2 Models

A Monte-Carlo radiative transfer model was used to compute the Stokes vector *(I, Q, U, V)* of the upwelling radiance just beneath the surface [15]. This model requires seven inputs: atmospheric Rayleigh optical depth, absorption and scattering of pure water (a_w and b_w, respectively), the water scattering phase matrix, $\mathbf{P_w}(\Theta)$, the particle-scattering phase matrix, $\mathbf{P_p}(\Theta)$, particulate scattering coefficient, b_p, and the absorption coefficient of dissolved and particulate constituents (a_{pg}).

The base model had the following input parameters: the Rayleigh optical depth of the atmosphere, τ_R, was computed from Tellet [16]. a_w and b_w were interpolated to NuRADS spectral bands from Table 1.1 in Pegau et al. [17]. $\mathbf{P_w}(\Theta)$ was given by Rayleigh scattering. Particle absorption (a_{pg}) and scattering (b_p) coefficients were derived from Morel and Gentili [18] using an estimated total Chlorophyll concentration of 0.1 μg / l and interpolated as necessary to the NuRADS spectral bands. Finally, $\mathbf{P_p}(\Theta)$ was a combination of the normalized Mueller matrix elements of Voss and Fry [19] and the Petzold scattering phase function [20]. The simulations were performed for a flat, plane, surface. Although wind speed measurements were not available for the measurement period, pictures taken during the measurement period showed the surface to be very flat, the wind speed is estimated to have been less than 2 m/s.

While investigating variations of this model, we also used a 1 term Henyey Greenstein (HG) phase function [21] and changed $\mathbf{P_p}(\Theta)$ to a reduced Rayleigh Mueller matrix with a depolarization ratio of 0.047 and 0.00 [22]. In addition we tried adding aerosols, using a maritime aerosol model [23], and also a rough surface using a Cox-Munk [24] formulation for the surface.

4. Results

4.1 Data

A sample PolRADS image is shown in Fig. 1. In the radiance image the anti-solar point has been marked by a white box. The rays emanating from this position are due to wave focusing. These images are in a fisheye projection where the center of the images is the nadir direction, the edge of the circle is the horizon, and the nadir angle varies linearly with radius from the center (nadir angle 0°) to the edge (nadir angle 90°). On the left, the ship and its direct shadow, can be seen right at the horizon. All data were taken with the ship more than 15-20 m away, however in this clear water the ship is still evident. On the right side of the image one can see a dome window from one of the other cameras. The general pattern of the upwelling radiance and the normalized stokes vector components *Q/I* and *U/I* can be seen from these images.

Figure 2 shows the average *Q/I* and *U/I* for the same period as the single image in Fig. 1. Also shown in Fig. 2 are the standard deviations for *Q/I* and *U/I*. As seen, the standard deviation is less than 0.05 over most of the image, often less than 0.02. As the average is made from several individual images, this standard deviation is dominated by the natural noise in the light field caused by surface waves and other environmental effects. The intrinsic instrument noise is much less than this, on the order of 0.02 or less.

#138994 - $15.00 USD Received 30 Nov 2010; revised 18 Feb 2011; accepted 8 Mar 2011; published 16 Mar 2011

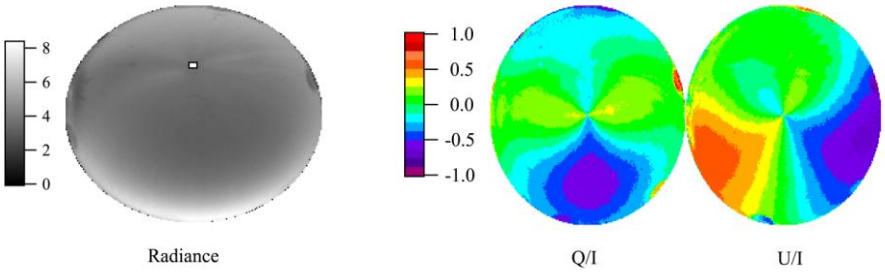

Fig. 1. Upwelling radiance (left) and *Q/I* and *U/I* for this image. The radiance units are μW cm^{-2} nm^{-1} sr^{-1}, *Q/I* and *U/I* are dimensionless. This was collected off of Hawaii (December 12, 2005, 20.83° N, 157.18° W, 10:25 local time). The wavelength was 436 nm and the solar zenith angle was 51°.

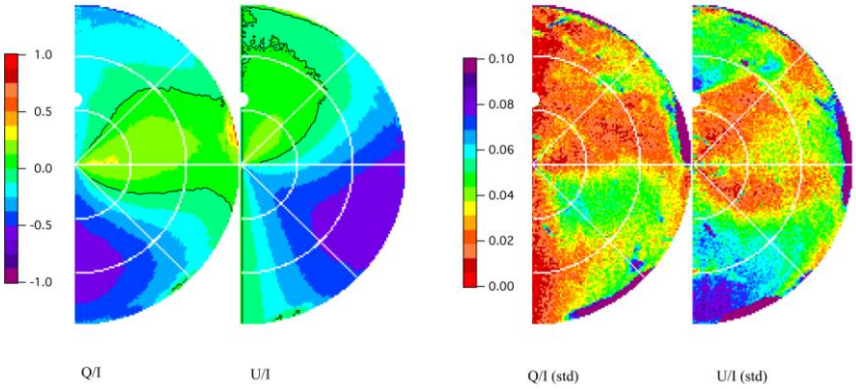

Fig. 2. Averaged data corresponding to data shown in Fig. 1. On the left, normalized stokes parameters *Q/I* and *U/I*. On the right is the standard deviation (SD) of the data points that constructed the mean images on the left. The SD is predominately less than 0.05 for most of the images. Also shown on these images, and the following images, are white lines depicting 30° and 60° nadir angles, and radial lines at azimuthal angles of 45°, 90°, 135°. The white circle on each is located at the refracted anti-solar position for reference. In the *Q/I* and *U/I* images, black lines are at *Q/I*=0 and *U/I*=0.

Figure 3 shows the *DOP* and the plane of polarization for the image shown in Fig. 2. A broad region of high polarization (above 50%) was observed on the solar side of the upwelling light field. On the anti-solar side of the light field there were the two regions of low polarization, which contain the neutral points. These were distinctly off of the principal plane (the plane containing the sun and zenith or nadir). Note that these points are also singularities in the plane of polarization field (points where the plane of polarization is not defined).

The neutral points were evident in the upwelling field, off of the principal plane, in the blue wavelengths. With our instrument we saw these at 412, 436, and 486 nm. At 526 nm they were evident sometimes but not always, and they degraded significantly above this wavelength. At longer wavelengths, the neutral points seemed to move towards the principal plane, but also it appeared that the wave effects, evident around the anti-solar point, became very important and introduced a lot of noise to the image. Figure 4 shows the degree of polarization for an image at 548 nm. In this it appears that one of the neutral points has moved to the anti-solar position, whereas there is still another point off of the principal plane, but at a much smaller nadir angle. There is actually a large area of very low polarization in this whole angular region.

Figure 5 shows the calculated azimuth and nadir angles of the neutral points measured on December 2 and 3, 2005. Nadir angle of 0° is viewing straight down, while azimuth angle of

#138994 - $15.00 USD Received 30 Nov 2010; revised 18 Feb 2011; accepted 8 Mar 2011; published 16 Mar 2011

0° is in the anti-solar direction. The positions were determined from calculating the intersection between the $Q = 0$ and $U = 0$ contour lines of the data. We used the 10 minute average data, discussed above, to reduce the noise in the images and the effects of the refracted solar beams. Points were excluded from Fig. 5 if the average *DOP* at the specific point, was greater than 1.5% (i.e. the minimum DOP was not zero thus not really a true neutral point). This included all the situations where the azimuth of the determined position was less then 15°. At the displayed positions, the minimum *DOP* was <1%, which is reasonably close to DOP=0, as would be expected at a neutral point, given the small errors in averaging and the expected instrument uncertainties.

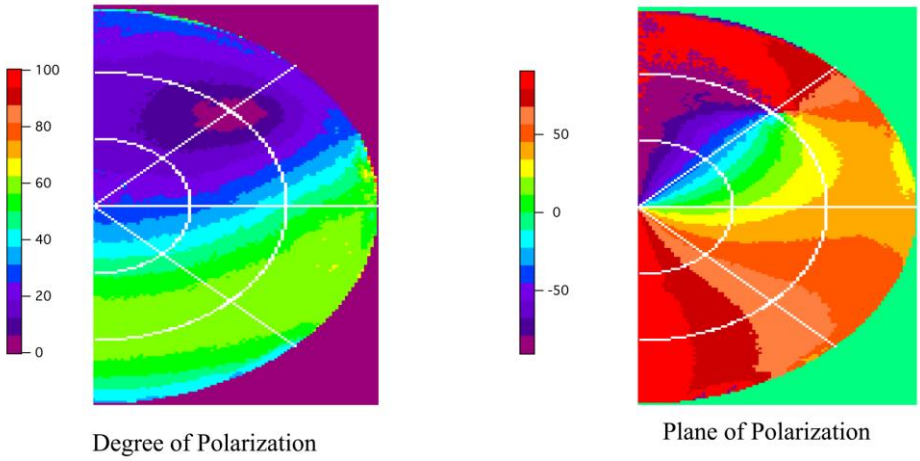

Fig. 3. Degree of polarization (*DOP*) and plane of polarization (χ) for image shown in Fig. 1. Color scales are shown for each image, *DOP* runs from 0 to 100%, while χ runs from –90° to 90°.

It can be seen that as one increases the wavelength from 412 nm to 526 nm, the neutral points vary both their nadir and azimuthal positions. Interestingly, at 412 nm the neutral points are far outside the "almucantar" of the anti-solar point (at greater nadir angle then the refracted anti-solar direction), while at 526 nm the neutral points move towards this almucantar. One can also see that the nadir angle increases with increasing solar zenith angle, while the azimuth position is relatively independent of the solar zenith angle.

For completeness, in Fig. 6 we show the maximum *DOP* (*DOPmax*) for these data sets, in the upwelling light field. These occur at approximately 90° scattering angle from the anti-solar point. As the wavelength increases from 412 nm to 526 nm, one sees an increase in the *DOPmax*. *DOPmax* at 412 nm is approximately 60%, while at 526 nm the *DOPmax* is closer to 70%. It can also be seen that as the solar zenith angle increases, the *DOPmax* decreases.

4.2 Model calculations

Before we discuss the results of the full Monte-Carlo calculations, including multiple scattering, it is useful to see what the simplest case would give. This would be a single scattering ocean, with only Rayleigh scattering, illuminated by the direct solar beam. Figure 7 shows *Q/I* and *U/I* for this simple case and a solar zenith angle of 50°. As discussed earlier, the neutral points in an image are at the points where the $Q/I = 0$ and $U/I = 0$ contour lines intersect. As can be seen in Fig. 7, the intersection of these two contour lines occurs at the anti-solar point and, uninterestingly because it is an artifact of the coordinate system, at the nadir. The real neutral point, at the anti-solar point, is always on the principal plane in the Rayleigh single scattering case. Multiple scattering is required to move the neutral points off of the anti-solar point, as for a purely Rayleigh scattering system illuminated only by a direct solar beam simple calculations show they are always on the principal plane. Even with the limitations of this simple system, it is useful to note how the single scattering case

#138994 - $15.00 USD Received 30 Nov 2010; revised 18 Feb 2011; accepted 8 Mar 2011; published 16 Mar 2011

qualitatively reproduces many of the features of the field data shown in Fig. 1 and can be used to understand the gross behavior.

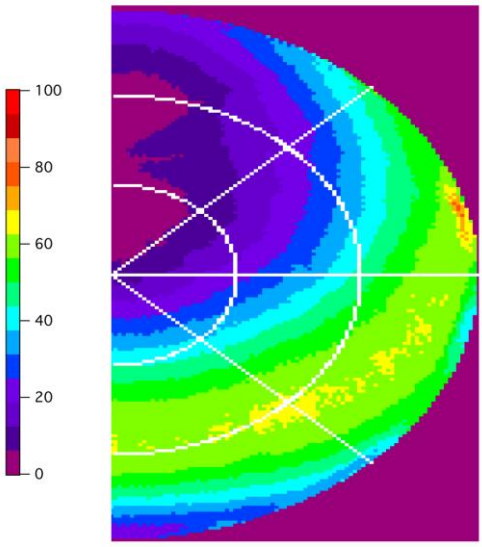

Fig. 4. Percent *DOP* illustrating large area of low polarization at 526 nm.

The total *Q/I* and *U/I* fields computed by Monte Carlo simulation can be separated into components due to the direct solar beam and due to diffuse skylight (Fig. 8). A comparison between Figs. 7, 8(a), and 8(d) suggests that the multiple scattering depolarizes the single scattered light field and alters the shapes of the *Q/I* and *U/I* neutral lines. In the direct beam case, $Q = 0$ and $U = 0$ contour lines intersect only on the principal plane, hence the neutral points will remain on the principal plane (Fig. 8a, d). In the diffuse (skylight) case, the intersection has moved off of the principal plane considerably (Fig. 8b, e) and are located at a nadir angle of 42° (outside the anti-solar point position of 35°) and an azimuthal position of 55°. In the combination of these two inputs, the total upwelling field, the neutral points do not move significantly off of the principal plane. This gives a strong indication that the effect we are seeing in our data is due to the diffuse sky radiance distribution. Off-axis neutral points, due to the diffuse input field, were also found in calculations by Chowdhary et al. [25] of the upwelling light field. Off-axis neutral points in the upwelling light field were also shown in a very recent paper by Adams and Gray [26], but only for very large solar zenith angles (example in [26] was at a solar zenith angle of 85°).

#138994 - $15.00 USD Received 30 Nov 2010; revised 18 Feb 2011; accepted 8 Mar 2011; published 16 Mar 2011

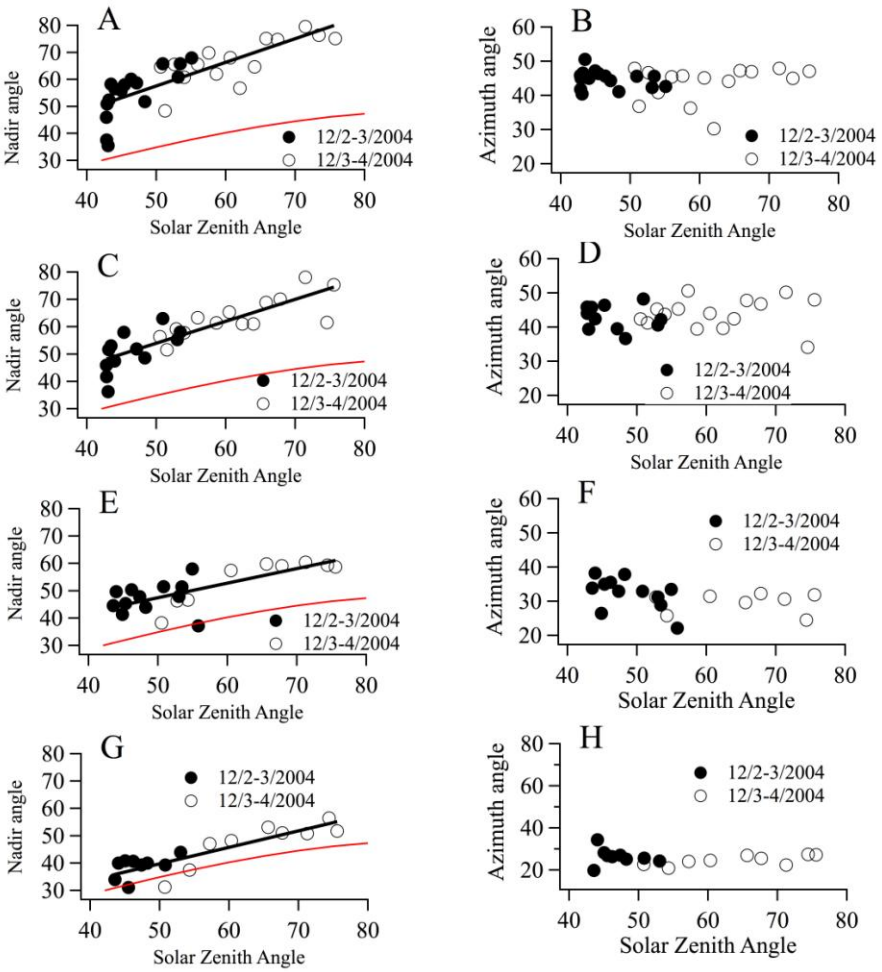

Fig. 5. Measured positions of neutral points. A, B correspond to 412 nm; C, D correspond to 442 nm; E, F correspond to 482 nm: G, H correspond to 526 nm. A, C, E, and G plot the nadir angle (0 is straight down). B, D, F, and H plot the azimuth angle (0 is in the anti-solar direction, so 45° corresponds to an azimuth of 135° with respect to the solar position. Lines in figures A, C, E, and G show the refracted solar position.

If the upwelling light fields due to the skylight and direct solar beam are added in different proportions, the neutral point positions smoothly vary from the direct beam case to this total skylight case. Interestingly, since τ_R is a strong inverse function of wavelength, the spectral trend in our data makes sense. We see (Fig. 5) that the experimentally observed neutral points are farthest off axis in the blue (more skylight), and move toward the principal plane in the red (less skylight).

5. Discussion

Since the model results did not agree with the measurements, we investigated several aspects of the data to verify the experimental results. As mentioned, in an earlier paper we performed an error analysis of the data processing inversion [12] and estimated that the uncertainty in the absolute value of the retrieved *Q/I* and *U/I* was approximately 0.05 and the accuracy of determining relative directions in the images is on the order of 1°. We studied the effect of globally changing *Q/I* and/or *U/I* by 0.05. Because we depend on the pattern of the *Q/I*=0 and *U/I*=0 more than the absolute value to determine the neutral point position, adding this error

#138994 - $15.00 USD Received 30 Nov 2010; revised 18 Feb 2011; accepted 8 Mar 2011; published 16 Mar 2011

to either or both of them did not significantly change the perceived location of the neutral points more than 2°-3° in azimuth or nadir angle. In addition, the addition of these factors significantly degraded the quality of the symmetry of the overall pattern, thus it is not likely that the error was this large.

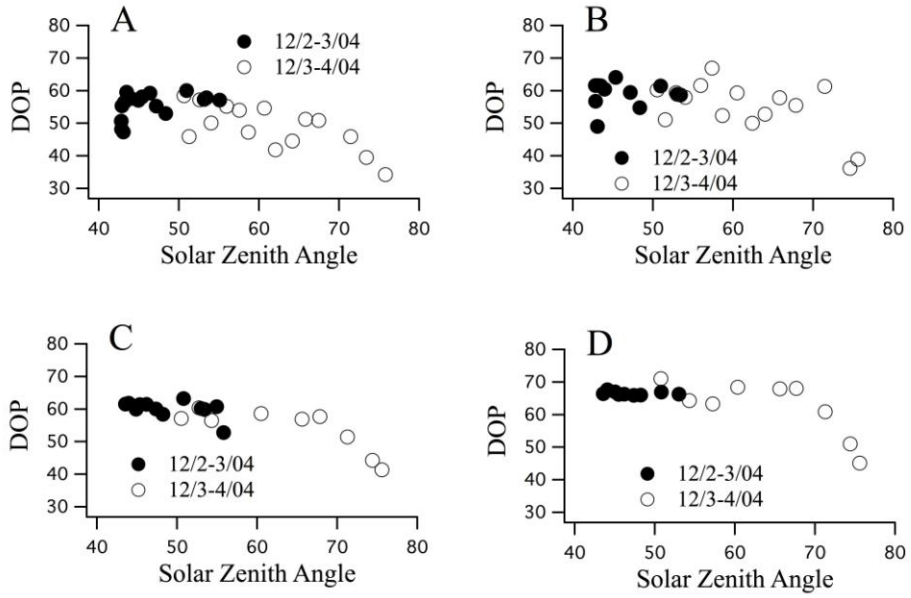

Fig. 6. Maximum *DOP* in images as a function of solar zenith angle A: 412 nm, B: 442 nm, C: 486 nm, and D: 526 nm. The maximum *DOP* can be seen to increase with increasing wavelength and decrease with increasing solar zenith angle.

Other possible sources of error in all in-water measurements include contamination by either instrument self shadow or shadowing by the ship. The polarization factors are determined by the balance of the measurements in the three PolRADS camera systems. The requirement for a low polarization value is a balance between the signals from the three separate cameras. Since each camera is in a separate housing as part of a triangle of camera systems, it is unlikely that each shadow would be the same, thus this effect would be more likely to increase the perceived degree of polarization rather than decrease it. In addition, the neutral points position off of the principal plane varied inversely to the water absorption and thus potential shadowing problems, hence this is not likely to be an instrument shadowing issue. Ship shadow could be an issue, but the instruments made their measurements over 20 m from the ship. In addition, as can be seen in the radiance image in Fig. 1, there was evidence of wave focusing effects around the anti-solar point, thus this area of the image (near the Neutral points) was clearly illuminated and not in the region of the ship shadow.

#138994 - $15.00 USD Received 30 Nov 2010; revised 18 Feb 2011; accepted 8 Mar 2011; published 16 Mar 2011

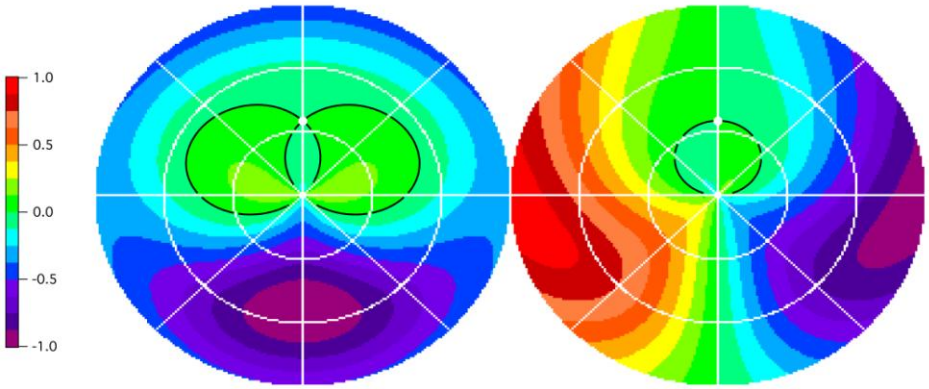

Fig. 7. *Q/I* and *U/I* shown for the case of single scattering, Rayleigh ocean, illuminated by a direct, unpolarized, solar beam. Also shown are black lines representing the *Q*=0 and *U*=0 contour lines for these images. This case is for a solar zenith angle of 50°.

Another possible source of error could be an error in our geometric location of the neutral points in our image. This was checked by looking at instrument features that can be seen in the unreduced data (such as the dome windows of the other cameras). The location of these features was calculated and found to agree with their physical location within 1°, so this error was discounted.

Other features of the polarized radiance distribution, such as the maximum DOP, agreed well with our calculations, so it was just these neutral points that resulted in a notable discrepancy between the model and the data. The neutral points are apparently very sensitive to water and atmospheric parameters that are difficult to model. Overall we could not find a reason to doubt the accuracy of these measurements.

With the models, many parameters were varied to try to reproduce the experiments. An HG phase function was used for the particulate scattering instead of the Petzold phase function, to allow a simple controllable shift to the shape of the phase function. We found that as we varied the asymmetry parameter in the HG phase function, the neutral point positions changed slightly. As this asymmetry parameter is decreased the neutral point moves closer to the principal plane, being on the principal plane for asymmetry parameters less than 0.1 and for a pure Rayleigh scattering case which has an asymmetry factor of 0.0. Nevertheless, using an asymmetry factor of 0.95 the neutral points are still very close to the PP with realistic atmospheric parameters.

We also investigated the effect of the index of refraction gradient at the air-sea interface. Contrary to the case for upwelling light above the ocean surface [8], the neutral points remain slightly off of the principal plane if the reflectance at the interface is “turned off” (index of water set to 1), as long as the HG asymmetry parameter is greater than 0.1.

We varied the aerosol optical depth (AOT). For an AOT less than 0.2, a large value for this maritime environment, there was no significant change in the calculated pattern. To look at the effect of a roughed surface, we used a wind-speed of up to 4 m/s, and although there was a disturbance to the pattern, the neutral point positions did not vary significantly.

We have also varied the sky polarized radiance distribution to see its effect on the neutral point positions. With an unpolarized, uniform skylight distribution, the only neutral point was at nadir. With an unpolarized sky having the same radiance distribution as the true Rayleigh sky, the neutral points were found only on the principal plane. In general, as the polarization of the Rayleigh sky was reduced, the neutral points due to skylight moved toward the principal plane. Therefore, the observation of off-principal plane neutral points apparently depends on both the intensity and polarization of the skylight radiance field.

#138994 - $15.00 USD Received 30 Nov 2010; revised 18 Feb 2011; accepted 8 Mar 2011; published 16 Mar 2011

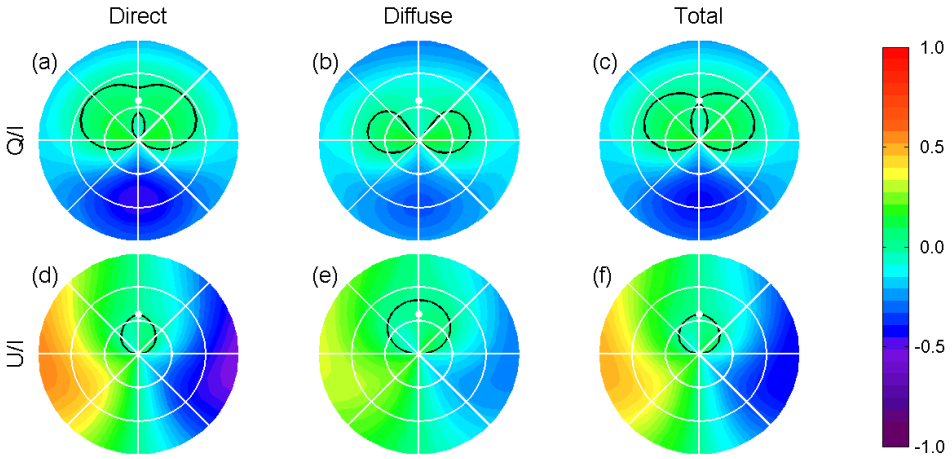

Fig. 8. Patterns of the *Q/I* (a-c), and *U/I* (d-f) parameters in the in-water upwelling radiance field. The system parameters are as described in Section 3.2. To take into account the aerosol, an aerosol layer of optical thickness 0.1 based on a maritime aerosol model [23] was included. Panel (a): contribution to the total *Q/I* field due to the direct sunlight (attenuated in the atmosphere); panel (b): contribution to the total *Q/I* field due to the diffuse skylight scattered in the atmosphere; and panel (c): the total *Q/I* field. The black lines are the contour lines of zero, i.e., the *Q* neutral lines. Panels d-f are similar to a-c, but for *U*.

6. Conclusions

We are not aware of any previous experimental observations of an in-water, off-principal plane neutral point. Our data showed that the position of this neutral point depended on the wavelength and solar zenith angle. Our model calculations could not move the neutral point to an angle significantly larger than the almucantor of the anti-solar point and therefore did not precisely replicate the experimentally observed positions of the off-principal plane neutral points. The model calculations did show, however, that skylight appears to strongly influence the location of these neutral points. Furthermore, the model calculations showed that strong polarization of the sky radiance distribution was required to move the neutral points off the principal plane. The positions of these neutral points are strongly influenced by the relative balance of the contribution of the irradiance due to the direct solar beam to that of the polarized skylight. As shown above, increases in attenuation of the direct solar beam due to aerosol or Rayleigh optical depth can move the neutral points off of the principal plane, as can very large solar zenith angles [26]. The position of the neutral points can be changed by the oceanic and atmospheric optical properties used in the radiative transfer models. The positions seem to be very sensitive to these input parameters, especially the aerosol and hydrosol scattering, so these measurement provide a sensitive test to the accuracy of these input parameters, and our understanding of the polarization in the upwelling light field. Further work needs to be done investigating these parameters to model this data set quantitatively.

Acknowledgements

This work was supported by NASA under grant NNX08AH93A (KV, AG, and HG). Development of the POLRADS instrument was supported by NASA grant NNG04HZ21C (KV). The Hawaii cruise data were collected with NASA support during a MOBY cruise, thanks to Dennis Clark (NOAA/NESDIS). The radiance distribution work and instrumentation development has been supported for many years by the Ocean Optics Program at ONR (KV, currently grant N00014-11-1-0153). GWK and YY's work was partially supported by ONR under grant N00014-08-1-0037.

#138994 - $15.00 USD Received 30 Nov 2010; revised 18 Feb 2011; accepted 8 Mar 2011; published 16 Mar 2011